University of Aden Journal of Natural and Applied Sciences., vol.30(1) (2026) 109 – 128

University of Aden Journal of Natural and Applied Sciences

Journal homepage: https://uajnas.adenuniv.com

Research Article

Modeling the Thermally Activated Mechanical Behavior of PVC

Yussra Fadhl Ali Qasem[1*] and Nadeem Mohammed Musahwar[2]

1 Department of Physics, Faculty of Education, University of Aden Yemen
2 Department of Physics, Faculty of Sciences, University of Aden, Yemen

https://doi.org/10.47372/uajnas.2026.n1.a07

ARTICLE INFO

Received: 30/04/2026

Accepted: 09/08/2026

Keywords:

Molecular Dynamics Simulation (MDS)
Unplasticized polyvinyl chloride (uPVC)
Mechanical Properties
CHARMM force field

Abstract

Unplasticized Polyvinyl Chloride (uPVC) is a vital structural thermoplastic whose macroscopic mechanical responses are governed by atomistic dynamics often inaccessible via traditional experimentation. This study aims to provide molecular-level insights into the macroscopic mechanical response and viscoplastic performance of amorphous uPVC. Atomistic Molecular Dynamics Simulations (MDS) were conducted using the Large-scale Atomic/Molecular Massively Parallel Simulator (LAMMPS) package and a reparametrized CHARMM force field. Amorphous simulated cells were equilibrated through a rigorous multi-stage thermal protocol within the Isothermal-Isobaric (NPT) ensemble. Uniaxial tensile tests were performed at a constant strain rate across temperatures ranging from 200 K to 350 K. Findings revealed that increasing temperature systematically reduced yield stress and significantly diminished material stiffness. Quantitative topological analysis demonstrated that initial elastic deformation is enthalpy-driven by non-bonded intermolecular interactions, whereas large strain hardening is entropy-driven, characterized by significant chain uncoiling and segmental alignment. This research establishes a predictive framework linking microstructural dynamics to macroscopic performance. The results confirm that elevated thermal energy facilitates molecular mobility and lowers energy barriers for conformational transitions, offering a robust contribution to the fundamental understanding of yield mechanisms in glassy thermoplastics and providing valuable insights for the design of polymer components under varying thermal conditions.

1. Introduction

Poly vinyl chloride (PVC) is a highly versatile thermoplastic material, currently ranking second only to polyolefins, specifically polyethylene (PE) and polypropylene (PP), in global production volume[1], [2]. Its widespread commercial significance directly results from its inherent properties and the capacity to modify them through formulation, allowing for an

*Corresponding author: Department of Physics, Faculty of Education- Aden, University of Aden Yemen
E-mail address: yussra500@gmail.com

unmatched range of applications[3]. Classified as a thermoplastic, PVC can be repeatedly softened by heating and hardened by cooling without undergoing significant chemical change, provided it is correctly formulated [3]. By varying the inclusion of plasticizers, the material transitions from a hard, brittle state, known as rigid or unplasticized PVC (uPVC), to a soft, pliable form, flexible PVC (PPVC), which significantly decreases the glass transition temperature (T_g) [4], [5]. This adaptability makes uPVC the most widely used polymer in the building and construction sectors for components such as rigid pipes and window frames, and the second most important polymer in automotive applications due to its high resistance to abrasion and excellent electrical insulation [6], [7].

The mechanical behavior of uPVC, particularly under tensile stress, is fundamental to its performance and safety in structural applications [8]. Tensile testing provides essential data regarding the mechanical response and resistance of the material, which is critical for engineering selection and design [9]. Under tensile loading, uPVC typically exhibits a characteristic plastic flow until fracture. This process features an initial linear elastic phase followed by a stress plateau and a subsequent strain hardening stage marked by an increase in stiffness [10], [11]. However, these macroscopic properties are heavily influenced by external factors such as strain rates, temperatures, and the material thermal or processing history [8], [10]. While traditional experimental methods effectively document the macroscopic results of a tensile test [8], they are often unable to elucidate why these phenomena occur at the atomistic level[12].

Molecular dynamics simulation (MDS) addresses this limitation by bridging the gap between macroscopic engineering observations and microscopic molecular physics [13], [14]. MDS enables the real-time observation of polymer chain dynamics, including stretching, alignment, and entanglement, which are the primary drivers of macroscopic tensile strength [15], [16]. This computational approach is particularly advantageous for investigating the behavior of glassy polymers during large deformations and strain hardening, as it allows for the precise control of variables, such as specific chain lengths and thermal histories, that are difficult to isolate in a laboratory setting [17-19].

The reliability of these simulations is intrinsically linked to the accuracy of the force field used to model interatomic interactions [12]. The CHARMM (Chemistry at Harvard Molecular Mechanics) force field is a widely recognized standard for modeling organic molecules and is inherently suitable for polymer systems like uPVC [20] . As a Class I force field, CHARMM represents the total potential energy as a summation of independent, additive

terms specifically harmonic potentials for bond stretching and angle bending, along with torsional dihedrals and non-bonded van der Waals and electrostatic interactions [21].

Unlike Class II force fields, this functional form omits complex cross-coupling terms, prioritizing computational efficiency and stability for large scale polymer systems. However, capturing the complex mechanical responses of polymer glasses, such as yielding and strain hardening, requires that these force fields are carefully validated against the specific glassy dynamics of the material [17], [22]. To bridge the gap between molecular topology and macroscopic performance, this study elucidates the atomistic deformation mechanisms governing uPVC tensile behavior. We employed Molecular Dynamics simulations (MDS) via LAMMPS, utilizing a reparametrized CHARMM force field optimized against experimental stress-strain data. Through simulated uniaxial tensile tests conducted across varying temperatures (200–350 K), this work establishes a comprehensive framework for understanding uPVC's mechanical response.

2. Computational Methodology

2.1. Potential Energy Function and Parameterization

The atomistic interactions in the amorphous uPVC system are governed by the CHARMM potential [23], where the total potential energy (U_{total}) is defined by the summation of bonded and non-bonded energy terms:

$$U_{total} = \sum_{bonds} K_b(b - b_0)^2 + \sum_{angles} K_\theta(\theta - \theta_0)^2 + \sum_{dihedrals} K_\phi[1 + \cos(n\phi - \delta)] + \sum_{i<j}\left[4\epsilon_{ij}\left(\left(\frac{\sigma_{ij}}{r_{ij}}\right)^{12} - \left(\frac{\sigma_{ij}}{r_{ij}}\right)^{6}\right) + \frac{q_i q_j}{4\pi\epsilon_0 r_{ij}}\right] \quad \text{.....(2.1)}$$

The intramolecular architecture is defined by three primary terms:1-Bond Stretching (U_{bond}): Represented by a harmonic potential where b_0 is the equilibrium bond length and K_b is the force constant. This term maintains the skeletal integrity of the C-C and C-Cl bonds under tensile loading [23] 2-Angle Bending (U_{angle}): Defined by the equilibrium angle θ_0 and the bending force constant K_θ .This term governs the resistance to chain straightening during the elastic deformation phase [23]. 3-Dihedral Torsion ($U_{dihedral}$): A periodic function describing the rotation about the polymer backbone. Here, $\emptyset$ is the dihedral angle, $K_\emptyset$ represents the torsional barrier height, n is the periodicity (multiplicity), and δ is the phase angle. This term is critical for capturing the trans-gauche conformational switching that characterizes plastic flow and energy dissipation [23], [24]. Non-bonded interactions are calculated for all atom pairs i and j separated by more than three bonds, encompassing the Lennard-Jones Potential (U_{LJ})

which accounts for van der Waals forces via the potential well depth(cohesive strength) ϵ_{ij} and the finite distance at which the interatomic potential is zero (effective atomic diameter) σ_{ij} [23] and Coulombic Potential ($U_{Coulombic}$) for long-range electrostatic interactions between partial atomic charges q_i and q_j separated by distance r_{ij}, with ϵ_0 representing vacuum permittivity [23].

When modeling the structural and mechanical properties of thermoplastics, CHARMM based all atom force fields are highly effective at reproducing equilibrium thermomechanical properties such as density, glass transition temperature (T_g), chain conformations, and small-strain elastic moduli provided they undergo polymer specific reparameterization [25] However, because standard CHARMM operates with a fixed bonding topology, it cannot natively model bond breaking, fragmentation, or chemically driven failure under high strain [26]. In contrast, reactive force fields like ReaxFF explicitly model reaction pathways and mechanochemistry, making them superior for studying fracture energetics, shock-induced degradation, and large-strain yielding where covalent bonds are severed [26], [27]. Meanwhile, other common nonreactive force fields, such as OPLS-AA, share similar capabilities and limitations with CHARMM. Both frameworks often require bespoke tailoring or even combination-as seen in mixed models like PLAFF3 to accurately capture the structural and thermomechanical behavior of specific polymers, with neither showing a definitive general advantage over the other for standard mechanical predictions [25].

To mitigate such discrepancies, reparameterization is essential to bridge the gap between atomic-level chemistry and macroscopic material behavior [28], [29]. This process categorizes coefficients into QM derived (Intramolecular) parameters including bond parameters (b_0, K_b), angles (θ_0, K_θ), and partial charges (q) are fixed based on DFT calculations (Hessian/ESP) [30]. This strictly preserves chemical identity and ensures the force field captures the true energetic cost of local deformations and chain rigidity [20] and experimentally tuned (Intermolecular/Torsional) parameters. Intermolecular forces, specifically the Lennard-Jones parameters controlling well depth and effective diameter (σ, ϵ), alongside backbone dihedrals (K_φ, n, δ), are adjusted to match macroscopic bulk observables [25]. While dihedrals are often initially fitted to QM baseline scans, they are fine-tuned alongside non-bonded terms to reproduce experimental PVT data; melt density, thermal expansivity, and T_g[31].

This macroscopic calibration of intermolecular interactions is critical, as sensitivity analyses demonstrate that these specific Lennard-Jones and torsional parameter adjustments directly control the predicted elastic modulus and yield stress of the thermoplastic [32].

Ultimately, the uPVC model is validated against three critical properties: density (ρ) (target $1.38 - 1.42 g/cm^3$ [33], controlled by atomic size (σ) [34], cohesive energy density (CED) (target $380 - 400\, J/cm^3$) [35], controlled by ϵ [36] and T_g (target $350 - 360K$) [37], controlled by backbone stiffness (K_φ)[31].

Non-bonded van der Waals interactions were computed using a potential switching scheme [38], employing an inner cutoff radius of 8 Å and an outer cutoff radius of 10 Å. This function ensures that both the potential and its first derivative vanish smoothly at the outer cutoff distance. A neighbor list skin distance of 2 Å was applied to update atom pairs efficiently. Long-range electrostatic interactions were resolved using the particle- particle- particle mesh (PPPM) solver [39] with a relative force accuracy of 10^{-4}.

2.2. Atomistic Model Construction

The construction of three-dimensional amorphous polymer systems was performed using the polymer builder module in CHARMM-GUI [40]. This module facilitated precise control over macromolecular structural parameters, including the degree of polymerization, chain count, and tacticity. For this study, isotactic (PVC) chains were generated with a polymerization degree of 80 monomers per chain. To ensure statistical reliability, simulation cells were constructed with varying dimensions, as detailed in Table 1.

Table 1: Structural details and composition of the as-prepared simulation cells, generated via the CHARMM package

Sample	1	2	3
Dimensions [Å]	$45 \times 45 \times 63$	$65 \times 65 \times 91$	$83 \times 83 \times 118$
Composition	PVC		
Type	Isotactic		
No. of monomers	80		
No. of chains	14	43	93
Simulated Density [g/cm^3]	1.44	1.44	1.44
Experimental Density [g/cm^3]	$1.3 - 1.58$ [42] ,[41] ,[2]		

2.3. Molecular Dynamics Simulation Protocol

All MDS were performed using the LAMMPS package [43], employing periodic boundary conditions in all three distinct directions. The equations of motion were integrated

with a time step of 2.0 fs. Temperature and pressure were regulated using the Nose-Hoover thermostat and barostat [44], [45], respectively, within the isobaric-isothermal (NPT) ensemble.

To eliminate high-energy artifacts and ensure a realistic amorphous density, the systems underwent a rigorous multi-stage thermal conditioning protocol: (1) initial 20 ns relaxation at 300 K and 0.987 atm; (2) During the second stage, each simulated cell was heated to 600K while maintaining the pressure at 0.987 atm over a period of 20 ns. (3) high-temperature equilibration at 600 K for 20 ns to randomize polymer conformations; (4) cooling to 100 K under an elevated pressure of 1.7 atm for 20 ns to enhance densification; and (5) final heating to target temperatures (200-350 K) and pressure relaxation to 0.987 atm over 40 ns.

Tensile properties were evaluated using non-equilibrium molecular dynamics (NEMD). Uniaxial deformation was applied along the z-axis using the LAMMPS deform command at constant strain rates of $5 \times 10^{9} s^{-1}$. During deformation, atomic velocities were remapped along the loading direction, while the transverse (x and y) boundaries were allowed to relax naturally.

3. Results and discussions

3.1 Structure of Simulated Samples

Post-processing and visualization were conducted using the OVITO (Open Visualization Tool) package [46]. The simulation trajectories were analyzed to assess domain homogeneity and verify the absence of structural artifacts. Quantitative characterization of short-range ordering was performed by calculating the radial distribution functions (RDF), while qualitative assessments focused on chain entanglement evolution and bond integrity under load.

The snapshots of some selected sample are shown in Figure (1a). All of the snapshots illustrated in our work are produced using OVITO software package. The atoms haven been colored based on their type as shown in the color scheme used in legends. For all simulated samples no crystalline regions have been observed. Hence, all of the simulated samples have amorphous structure. The samples show homogeneous distribution. The types of carbons atoms that form the backbones are illustrated in the legends. There is no evidence of cross-links formation between the backbones of neighboring chains. As regard the conformation of chains, the shown chain backbones in Figure (1b) reveals that chains exhibit a highly coiled conformation and there is no clear significant elongation and orientation for all simulated samples under equilibrium at 300K.

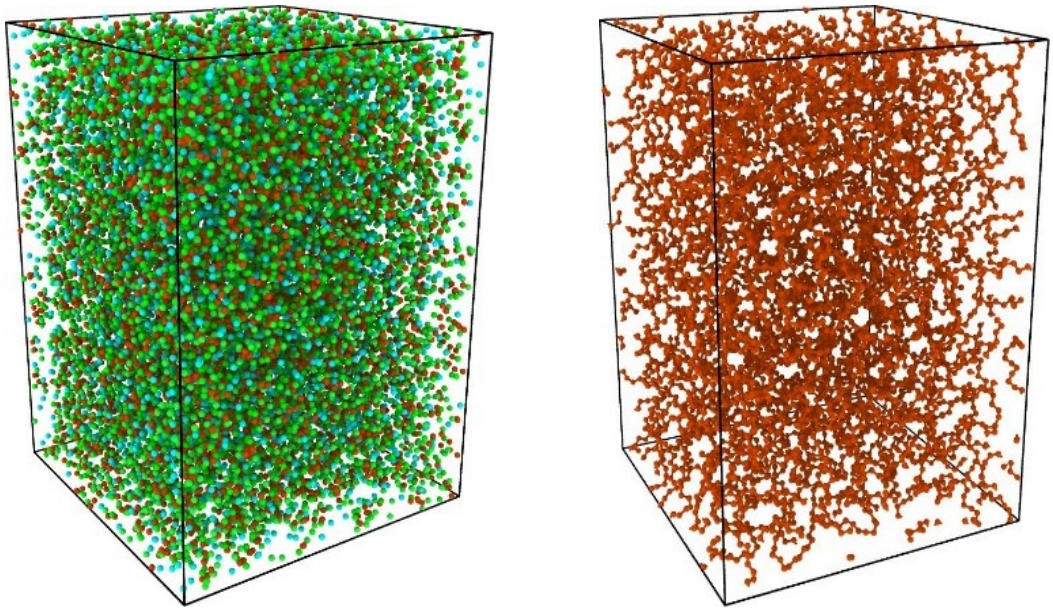

(a) (b)

Figure 1: (a)simulated sample PVC at 300k (b) The backbones of simulated sample PVC
H C Cl

The local structural environment of uPVC matrix was characterized using the RDF, $g(r)$, as illustrated in Figure 2. The RDF provides a quantitative measure of the probability of finding a particle at a distance r from a reference atom, effectively serving as a structural fingerprint of the short-range order within the amorphous polymer [47].

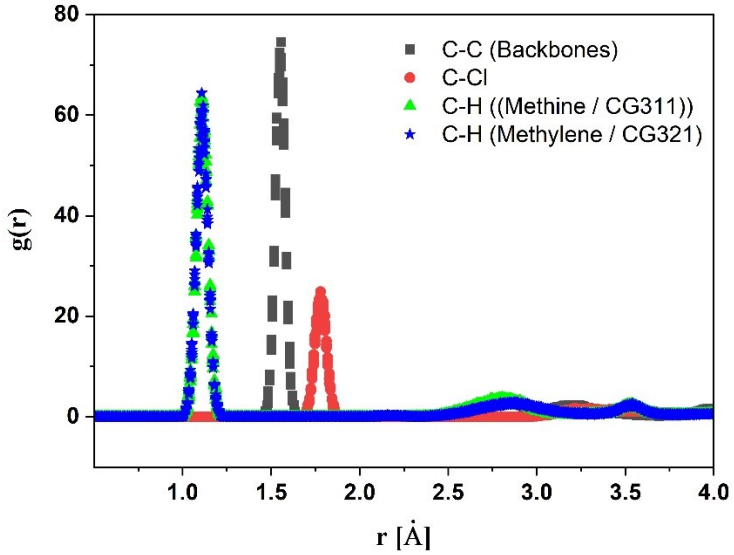

Figure 2: Radial Distribution Function (RDF), g(r), as a function of distance r(Å) for the primary atom pairs within the PVC matrix

The sharp, discrete peaks observed at low r values correspond to the primary covalent bonds within the uPVC chain architecture. The first peak, appearing at approximately 1.1 Å (represented by the green and blue curves), corresponds to the C-H stretching distance. The

secondary peak at 1.55 Å (black curve) represents the C-C backbone bond length, while the peak at 1.8 Å (red curve) identifies the C-Cl bond. These peak positions are in excellent quantitative agreement with established experimental values determined via gas-phase electron diffraction and high-resolution spectroscopy [48], [49]. The narrowness and high intensity (reaching values up to g(r) ≈ 75 for C-C) of these peaks indicate that the bonded distances are highly constrained and consistent across the simulation box, confirming the stability of the topological parameters utilized [50].

3.2. System Stability and Cell Validation

The initial stage of thermal conditioning protocol focused on confirming the thermodynamic stability of the amorphous glass to ensure that the tensile data reflects a physical state free from structural artifacts. As shown in Figure 3, the density and total potential energy were monitored over a sequence of time steps at 300 K and 0.987 atm, which is a standard approach for verifying particle system equilibrium [39]. The density trajectory (left axis) shows a rapid convergence within the first 100 ps, and simultaneously, the potential energy (right axis) exhibits a sharp initial decline as the system relaxes from its initial random packing. Following this, both the density and the total potential energy exhibit standard thermal fluctuations over time. Crucially, these values fluctuate consistently around a stable average, which is the primary indicator that the system has successfully reached thermodynamic equilibrium and that the internal stresses have been relaxed. To quantitatively demonstrate this stability, the standard deviation for the production phase of the simulation was calculated. The system stabilizes at an average density of 1.345 ± 0.0015 g/cm³ which aligns closely with the experimental density for rigid PVC [35] and a total potential energy of 86,661 ± 170 kcal/mol. Although the curves display instantaneous oscillations which are a characteristic physical response of the Nose-Hoover algorithms used to maintain temperature and pressure, the extremely low standard deviations relative to the average values confirm that the structural relaxation is complete. The absence of a continuous energy drift confirms that the system has successfully navigated local energy minima to reach a relaxed, metastable glassy state suitable for deformation studies [47].

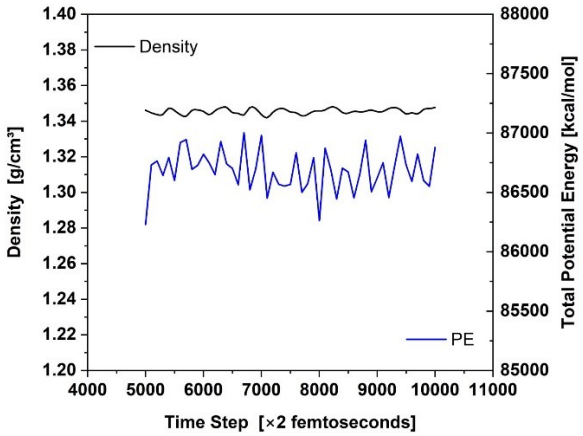

Figure 3: Equilibration trajectory showing the stabilization of density (left axis) and potential energy (right axis) for the PVC model at 300 K.

To ensure that the results were not influenced by periodic boundary conditions, the influence of simulation box dimensions was evaluated. Figure 4 illustrates the true stress-strain curves for four cell sizes. The smallest cell shows significant stress fluctuations and an overestimation of the yield peak, likely due to the periodic images constraining the natural development of shear bands [51], [52]. However, for the biggest simulation cells ($83 \times 83 \times 118 Å^3$ and $105 \times 105 \times 153 Å^3$), the stress-strain profiles overlap almost perfectly, particularly in the post-yield flow region. This convergence validates that the larger cells act as a representative volume element (RVE) capable of capturing the collective molecular rearrangements, or shear transformation zones, necessary for bulk property prediction [22]. Hence the chosen simulation cell size was $83 \times 83 \times 118 Å^3$, the choice which reduce the computational cost.

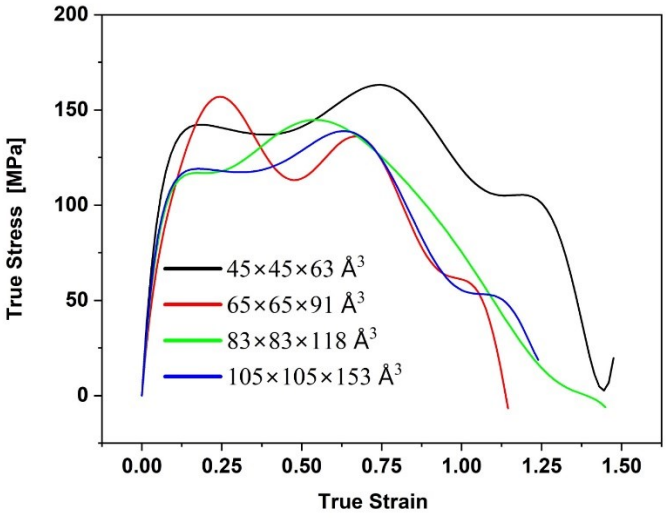

Figure 4: Effect of simulation box size on the uniaxial tensile response of glassy PVC

3.3. Macroscopic Mechanical Behavior

The mechanical behavior of the simulated uPVC system is highly sensitive to thermal conditions, as demonstrated by the true stress-strain curves presented in Figure 5. The figure illustrates the tensile response at four different temperatures (200 K, 250 K, 300 K, and 350 K) under a constant applied strain rate of $5\times 10^{9}s^{-1}$. Across all temperature profiles, the material exhibits the characteristic sequence of a glassy polymer undergoing large inelastic deformation: an initial linear elastic region, a distinct yield peak, a period of strain softening, and a concluding strain-hardening phase.

Figure 5 demonstrates that increasing temperature from 200 K to 350 K systematically reduces stress across all deformation stages. In the initial elastic range, the linear slope decreases as temperature rises, indicating a significant reduction in material stiffness. This trend continues into the yield region, where the peak stress drops significantly from approximately 250 MPa at 200 K to nearly 100 MPa at 350 K. Following yield, the magnitude of strain softening decreases with rising temperature, and the subsequent strain hardening regime shifts downward. Consequently, while the material continues to harden at larger strains, the overall flow stress at 350 K remains consistently lower than the levels observed at 200 K.

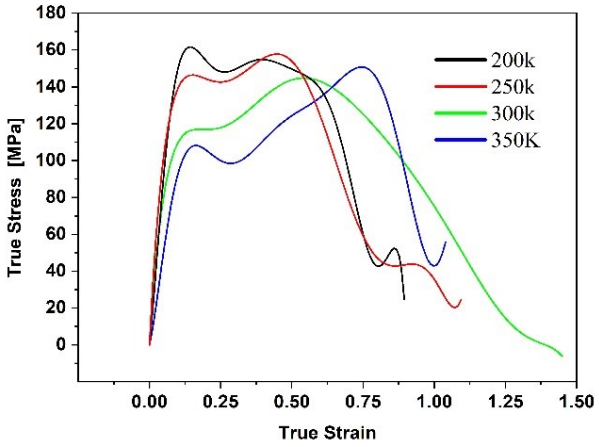

Figure 5: True stress-strain behavior of amorphous uPVC under uniaxial tension at temperatures ranging from 200 K to 350 K ($5\times 10^{9}s^{-1}$)

3.4. Structural and Topological Evolution

The analysis of the microstructural evolution of the uPVC system during uniaxial deformation is illustrated in Figure 6, which tracks four critical parameters: the radius of gyration (R_g), the end-to-end distance (R_{ee}), Herman's orientation factor (f), and the fractional free volume (FFV). These descriptors provide a molecular-scale explanation for the macroscopic mechanical transitions observed in the stress-strain profiles.

Figures 6a and 6b illustrate the evolution of chain dimensions during deformation and their dependence on temperature from 200 K to 350 K. In the elastic range, both the R_g in Figure 6a and the R_{ee} in Figure 6b remains relatively constant, as small-strain deformation primarily involves bond stretching rather than large-scale chain reconfiguration. As the material reaches the yield point and enters Strain Softening, both R_g and R_{ee} begin to increase, signaling the onset of permanent molecular displacement. This growth is most pronounced in the strain hardening regime, where chains undergo significant conformational uncoiling and alignment. Temperature plays a critical role here: at higher temperatures (350 K), the chains exhibit greater mobility, leading to a more rapid increase in R_g and R_{ee} at lower stress levels compared to the 200 K state. Conversely, at lower temperatures, the restricted mobility requires higher stress to achieve the same degree of chain extension.

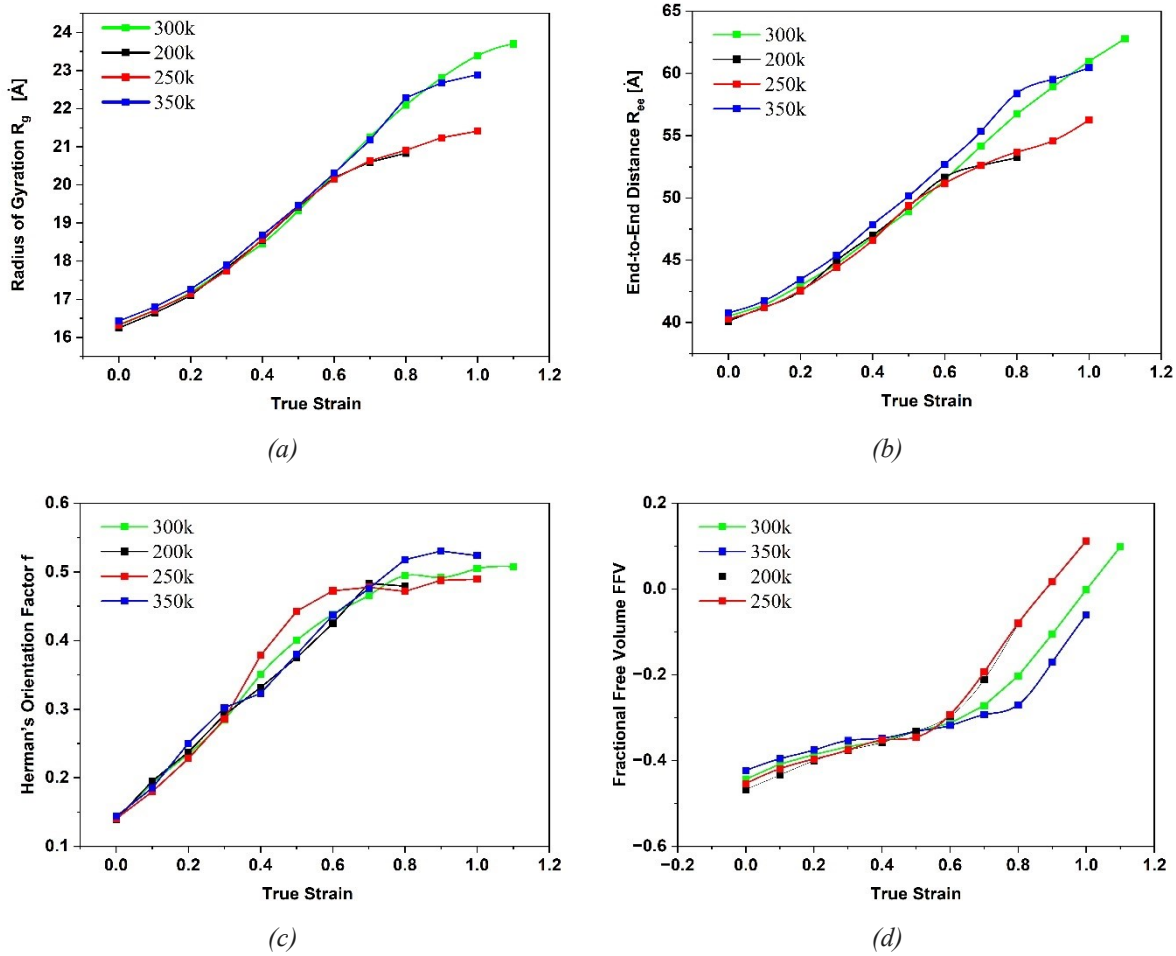

Figure 6: Evolution of the chain's global dimensions as a function of true strain across different temperatures: (a) Radius of gyration (R_g), and (b) End-to-end distance (R_{ee}) (c) Herman's Orientation Factor f (d) Fractional Free Volume (FFV)

As shown in figure 6c, in the elastic range, f remains near zero as deformation is limited to bond stretching without large-scale chain movement. Upon reaching the yield point, f begins to rise, signaling the onset of permanent molecular alignment. During strain softening and strain hardening, orientation increases continuously as chains uncoil and align with the stretching direction. Higher temperatures significantly facilitate this process; at 350 K, the orientation factor reaches higher values at equivalent strains compared to 200 K, as increased thermal energy lowers the energy barriers for segmental rotation. The evolution of FFV during uniaxial stretching is presented in Figure 6d, in the elastic range, FFV is stable, though the baseline is higher at 350 K due to thermal expansion. At the yield point, FFV begins to increase as the material dilates to accommodate flow. A sharp uptick occurs during strain softening. In the strain hardening regime, a temperature inversion is observed: the lower temperature curves (200 K and 250 K) eventually reach higher FFV levels at large strains than the 350 K curve.

3.5. Energetic Contributions and Mechanisms

The mechanical behavior of thermoplastics is governed by a complex energy landscape involving the storage, dissipation, and transformation of internal energy across molecular scales [24]. These materials bridge the gap between macroscopic mechanical behaviors, such as yielding and necking, and microscopic molecular dynamics. Thermoplastic molecules consist of long macromolecular chains with a strong covalent backbone of carbon atoms. While atoms within a chain are linked by intense covalent bonds, the interactions between separate chains are dictated by much weaker non-bonded forces, such as van der Waals or hydrogen bonds. The total energy of the system is the sum of bonded interactions (stretching, bending, and torsion) and non-bonded interactions [23].

Figures 7a-d depict the evolution of bond stretching (7a), bond bending (7b), dihedral rotational (7c), and non-bonded (7d) energies during deformation. Across all figures, higher temperatures (300 K, 350 K) establish a significantly higher absolute initial energy baseline due to greater thermal kinetic energy. In the elastic range, the covalent energies (stretching, bending, dihedral) experience minor fluctuations as deformation relies on small scale affine displacements. Meanwhile, non-bonded energy increases sharply across all temperatures as intermolecular distances expand. This rise is particularly steep at 200 K due to the densely packed, rigid nature of the colder matrix. Upon reaching the yield point, the energetic transition is heavily temperature-dependent. At lower temperatures (200 K, 250 K), forcing the restricted glassy matrix to yield causes abrupt shifts in conformational energies (bending and dihedral) compared to the smoother, thermally-assisted transitions observed at 350 K.

During strain softening, dihedral and bending energies generally decrease as chains overcome localized barriers and reorganize into conformations that more easily accommodate flow. This energy drop is more severe at 200 K, reflecting the breakdown of its initially high structural resistance. The non-bonded energy continues to rise during this stage but its rate of change begins to decelerate. In the strain hardening regime, covalent energies exhibit gradual downward trends or fluctuations as large-scale chain alignment occurs. The non-bonded energy reaches a maximum and then slightly decreases. The temperature influence remains prominent: the enhanced molecular mobility at 350 K allows the polymer network to accommodate massive, high-strain deformation with relatively stable, smooth energetic transitions. Conversely, the 200K and 250 K profiles display more severe, localized energetic variations, underscoring the significant internal resistance of the cold polymer network.

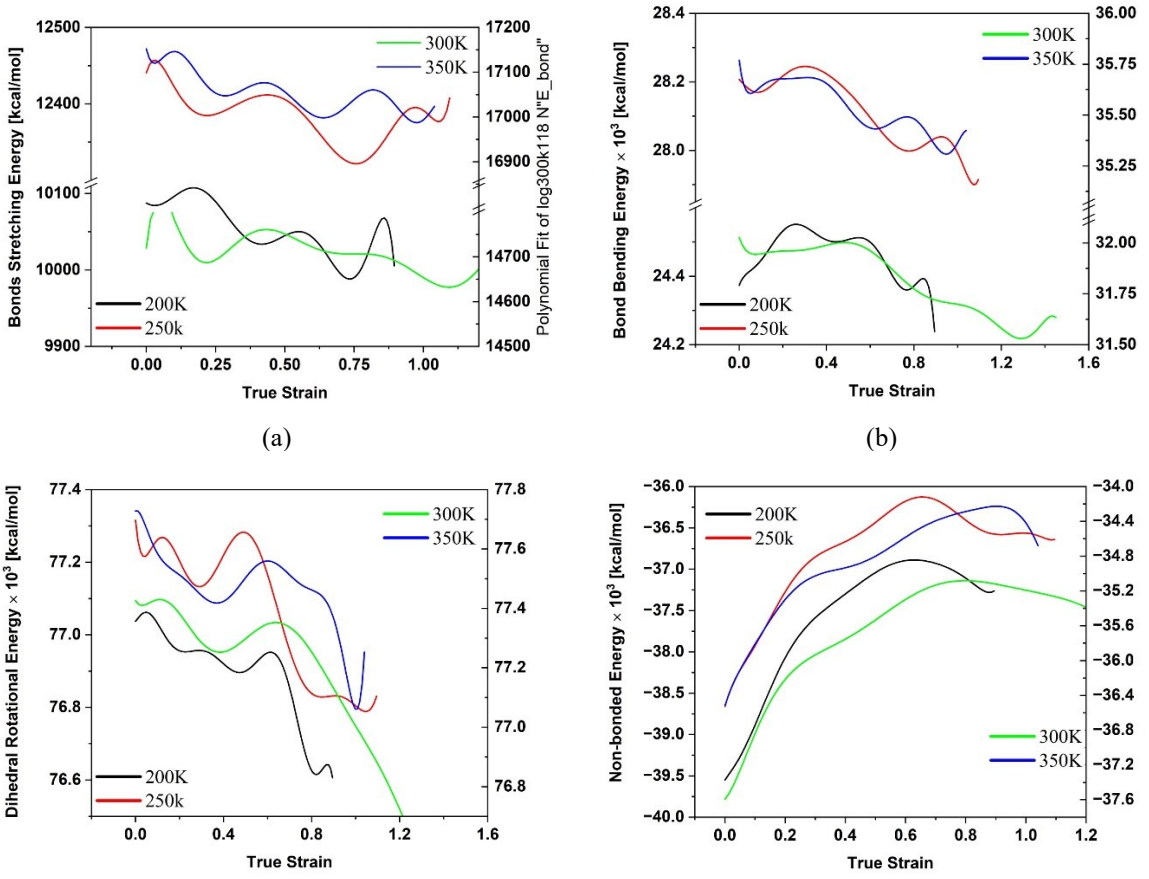

Figure 7: Molecular Bond Energy for uPVC at a strain rate of 5 $\times 110^{9}s^{-1}$and different temperatures: (a) Bond stretching energy, (b) Bond bending energy, (c) Dihedral energy, and (d) non-bonded energy

3.6. Multi-Scale Correlation of Macroscopic Deformation and Atomistic Mechanisms

The mechanical response of the thermoplastic reflects a complex transition from energy-driven to entropy-driven resistance (as established in the stress-strain profiles of(Figure 5). In the initial elastic region, the material's stiffness is primarily governed by changes in internal energy rather than entropy. Small-strain elasticity relies on the resistance of the polymer network to affine bond distortion, setting the initial slope of the stress-strain curve [53]. This initial modulus is dominated by intermolecular Van der Waals forces rather than covalent interactions. This mechanism is verified by the energetic evolutions, where covalent bond stretching and bending energies exhibit minimal fluctuations (Figures 7a and 7b), while non-bonded energy rises sharply as mechanical work forces segments apart against cohesive interactions (Figure 7d). Furthermore, as the temperature increases to 350 K, thermal expansion increases the baseline molecular spacing and fractional free volume [54]. This expanded state weakens the cohesive energy density, resulting in a noticeably lower initial modulus compared to the denser, rigid 200 K matrix.

The transition from elastic behavior to plastic yielding is characterized by a significant peak stress that drops sharply at higher temperatures. According to Eyring's theory of thermally activated flow, polymer segments are trapped in local energy minima. Yielding acts as a stress-biased process where temperature provides the necessary kinetic energy to overcome these internal barriers [55], [56]. Consequently, at 350 K, the abundant thermal energy ensures that far less mechanical stress is required to trigger yielding. Microscopically, this transition to a plastic state is driven by structural dilation, where local voids open to accommodate flow, accompanied by the breakdown of the isotropic glassy state and the onset of permanent segmental alignment [57]. These structural shifts are confirmed by the immediate growth in FFV (Figure 6d) and the initial rise in Herman's orientation factor (Figure 6c) at the yield point.

Following the yield peak, the material undergoes strain softening, a distinct stress drop driven by a rapid increase in molecular mobility and structural dilation. This effectively lowers the nucleation energy required for localized shear transformations to activate [54], [57], [58]. The dilation facilitates necessary conformational transitions, allowing polymer chains to overcome localized steric barriers and rotate into lower energy conformations that more easily accommodate plastic flow. This theoretical conformational shift is corroborated by the observed drop in dihedral rotational energies during this phase (Figure 7c). This softening effect is significantly more severe at 200 K because the initially dense matrix requires an abrupt,

mechanically forced structural breakdown, whereas the 350 K state transitions more smoothly due to its pre-existing high thermal mobility.

At large strains, the material enters the strain hardening regime, where stress begins to rise again due to entropic network resistance. In their undeformed state, flexible polymer chains exist as randomly tangled coils representing a state of maximum entropy [57]. As they are extended during macroscopic deformation, the chains physically uncoil and stretch, aligning with the loading axis. This decreases the number of possible configurations, resulting in a low-entropy state where the polymer network thermodynamically resists further extension [57]. This macroscopic hardening is validated at the micro-scale by massive, sustained increases in the radius of gyration and end-to-end distance (Figures 6a and 6b), alongside Herman's orientation factor reaching its peak values (Figure 6c) [59]. Finally, the entire strain hardening regime shifts downward at higher temperatures because elevated thermal energy increases segmental mobility. This allows chains to slide and reconfigure more efficiently during stretching, preventing the buildup of high internal stresses.

4. Conclusions

This study successfully established a Molecular Dynamics framework to elucidate the atomistic origins of the macroscopic mechanical behavior of uPVC. Utilizing a reparametrized CHARMM force field alongside a rigorous multi-stage thermal conditioning protocol, the system achieved a stable glassy state with a converged density of 1.345 g/cm^3, accurately matching experimental benchmarks. The use of an optimized Representative Volume Element ensured that localized plastic events, such as Shear Transformation Zones, were captured without periodic boundary artifacts.

With the system validated, the model effectively reproduced the characteristic viscoplastic deformation profile of uPVC encompassing linear elasticity, yield peak, strain softening, and strain hardening across a comprehensive temperature range of 200 K to 350 K. By bridging macroscopic observations with micro-scale evidence, the simulations revealed that small-strain elasticity is primarily enthalpy-driven, whereas large-strain hardening is strictly entropy-driven, as marked by substantial increases in the radius of gyration and end-to-end chain distance. Furthermore, tracking the fractional free volume and Herman's orientation factor successfully linked structural dilation and segmental alignment to the onset of plastic flow, confirming the model's alignment with Eyring's theory of thermally activated flow.

While the framework expertly captures the viscoplastic drawing and orientation of the polymer network, its fundamental limitation stems from the non-reactive nature of the CHARMM force field. Because it operates with fixed bonding topologies, the simulation cannot predict chemical bond scission, macromolecular fragmentation, or mechanochemically driven fracture. Ultimately, the model developed in this study provides a powerful and highly successful tool for analyzing non-destructive mechanical behavior, pre-yield dynamics, and complex flow regimes where covalent bond integrity is maintained.

References

[1] D. Braun, "Poly (vinyl chloride) on the way from the 19th century to the 21st century," *J. Polym. Sci. A Polym. Chem.*, vol. 42, no. 3, pp. 578–586, Feb. 2004, doi: 10.1002/pola.10906.

[2] W. D. Callister and D. G. Rethwisch, *Materials science and engineering: an introduction*, 10th ed. John Wiley & Sons, 2018.

[3] S. G. Patrick, *Practical Guide to Polyvinyl Chloride*, 1st ed. UK: Rapra Technology Limited, 2005.

[4] F. C. Amorim, J. F. B. Souza, H. S. da Costa Mattos, and J. M. L. Reis, "Temperature effect on the tensile properties of unplasticized polyvinylchloride," *SPE Polymers*, vol. 3, no. 2, pp. 99–104, Apr. 2022, doi: 10.1002/pls2.10067.

[5] K. G. Alahapperuma and A. M. P. B. Samarasekara, "Degradation of unplasticised poly vinyl chloride based engineering products upon exposure to ultra violet radiation," *Tropical Agricultural Research*, vol. 30, no. 4, p. 117, Nov. 2019, doi: 10.4038/tar.v30i4.8333.

[6] C. M. R. Abreu, A. C. Fonseca, N. M. P. Rocha, J. T. Guthrie, A. C. Serra, and J. F. J. Coelho, "Poly(vinyl chloride): current status and future perspectives via reversible deactivation radical polymerization methods," *Prog. Polym. Sci.*, vol. 87, pp. 34–69, Dec. 2018, doi: 10.1016/j.progpolymsci.2018.06.007.

[7] A. Hameed and Z. G. M. Salih, "A Study of some Mechanical Behavior on a Thermoplastic Material," *Journal of Al-Nahrain University*, vol. 14, no. 3, pp. 58–65, 2011.

[8] N. A. Saad, M. H. Al-Maamory, M. R. Mohammed, and A. A. Hashim, "The Effect of Several Service and Weathering Parameters on Tensile Properties of PVC Pipe Materials," *Materials Sciences and Applications*, vol. 03, no. 11, pp. 784–792, 2012, doi: 10.4236/msa.2012.311114.

[9] N. Akel, G. Stoltz, A. Wautier, F. Nicot, and N. Touze, "Rate-dependent tensile response of Polyvinyl Chloride geomembranes," *International Journal of Geosynthetics and Ground Engineering*, vol. 53, no. 1, pp. 445–456, 2025, doi: 10.1016/j.geotexmem.2024.11.004.

[10] G. Pezzin, G. Ajroldi, T. Casiraghi, C. Garbuglio, and G. Vittadini, "Dynamic-mechanical and tensile properties of poly(vinyl chloride). Influence of thermal history and crystallinity," *J. Appl. Polym. Sci.*, vol. 16, no. 7, pp. 1839–1849, Jul. 1972, doi: 10.1002/app.1972.070160720.

[11] A. S. Ognedal, "Large-Deformation Behaviour of Thermoplastics at Various Stress States: An experimental and numerical study," *Norwegian University of Science and Technology*, 2012.

[12] C. Li and A. Strachan, "Molecular scale simulations on thermoset polymers: A review," *J. Polym. Sci. B Polym. Phys.*, vol. 53, no. 2, pp. 103–122, Jan. 2015, doi: 10.1002/polb.23489.

[13] M. P. Allen, "Introduction to molecular dynamics simulation," in *Computational Soft Matter: From Synthetic Polymers to Proteins, 23*, vol. 23, N. Attig, k. Binder, H. Grubmuller, and K. Kremer, Eds., John von Neumann Institute for Computing, 2004, pp. 1–28.

[14] S. Sharma, P. Kumar, and R. Chandra, *Introduction to Molecular Dynamics*. Elsevier, 2019. doi: 10.1016/C2017-0-04396-3.

[15] I. H. Sahputra and A. T. Echtermeyer, "Effects of temperature and strain rate on the deformation of amorphous polyethylene: a comparison between molecular dynamics simulations and experimental results," *Model. Simul. Mat. Sci. Eng.*, vol. 21, no. 6, p. 065016, Aug. 2013, doi: 10.1088/0965-0393/21/6/065016.

[16] V. M. Nazarychev, A. V. Lyulin, S. V. Larin, A. A. Gurtovenko, J. M. Kenny, and S. V. Lyulin, "Molecular dynamics simulations of uniaxial deformation of thermoplastic polyimides," *Soft Matter*, vol. 12, no. 17, pp. 3972–3981, 2016, doi: 10.1039/C6SM00230G.

[17] D. M. Anstine, A. Strachan, and C. M. Colina, "Effects of an atomistic modeling approach on predicted mechanical properties of glassy polymers via molecular dynamics," *Model. Simul. Mat. Sci. Eng.*, vol. 28, no. 2, 2020, doi: 10.1088/1361-651X/ab615c.

[18] Z. Zhang, L. Zhang, J. Jasa, W. Li, G. Gazonas, and M. Negahban, "High fidelity computational characterization of the mechanical response of thermally aged polycarbonate," *Model. Simul. Mat. Sci. Eng.*, vol. 25, no. 5, p. 055012, Jul. 2017, doi: 10.1088/1361-651X/aa7341.

[19] W. Tao *et al.*, "Strain rate and temperature dependence of the mechanical properties of polymers: A universal time-temperature superposition principle," *J. Chem. Phys.*, vol. 149, no. 4, Jul. 2018, doi: 10.1063/1.5031114.

[20] K. Vanommeslaeghe *et al.*, "CHARMM general force field: A force field for drug-like molecules compatible with the CHARMM all-atom additive biological force fields," *J. Comput. Chem.*, vol. 31, no. 4, pp. 671–690, Mar. 2010, doi: 10.1002/jcc.21367.

[21] A. D. MacKerell *et al.*, "All-Atom Empirical Potential for Molecular Modeling and Dynamics Studies of Proteins," *J. Phys. Chem. B*, vol. 102, no. 18, pp. 3586–3616, Apr. 1998, doi: 10.1021/jp973084f.

[22] J. L. Barrat, J. Baschnagel, and A. Lyulin, "Molecular dynamics simulations of glassy polymers," *Soft Matter*, vol. 6, no. 15, pp. 3430–3446, Jul. 2010, doi: 10.1039/b927044b.

[23] B. R. Brooks, R. E. Bruccoleri, B. D. Olafson, D. J. States, ; S Swaminathan, and M. Karplus, "CHARMM: A Program for Macromolecular Energy, Minimization, and Dynamics Calculations*," 1982. doi: https://doi.org/10.1002/jcc.540040211.

[24] A. S. Argon, "The physics of deformation and fracture of polymers," in *The Physics of Deformation and Fracture of Polymers*, Cambridge University Press, 2013, ch. 12, pp. 391–434. doi: 10.1017/CBO9781139033046.014.

[25] J. H. McAliley and D. A. Bruce, "Development of Force Field Parameters for Molecular Simulation of Polylactide," *J. Chem. Theory Comput.*, vol. 7, no. 11, pp. 3756–3767, Nov. 2011, doi: 10.1021/ct200251x.

[26] T. Panczyk, K. Nieszporek, and P. Wolski, "Modeling the degradation of polypropylene and polystyrene under shock compression and mechanical cleaving using the ReaxFF force field," *Chemosphere*, vol. 357, p. 142056, Jun. 2024, doi: 10.1016/j.chemosphere.2024.142056.

[27] L. Liu and G. Raos, "Assessment of reactive force fields for the failure of hydrocarbon chains: Insights from molecular dynamics and density functional theory," *Polymer (Guildf).*, vol. 348, p. 129732, 2026, doi: 10.1016/j.polymer.2026.129732.

[28] G. M. Odegard, T. C. Clancy, and T. S. Gates, "Modeling of the mechanical properties of nanoparticle/polymer composites," *Polymer (Guildf).*, vol. 46, no. 2, pp. 553–562, Jan. 2005, doi: 10.1016/j.polymer.2004.11.022.

[29] R. Simões, J. Viana, G. R. Dias, and A. M. Cunha, "Influence of the Interaction Potential Parameters on the Mechanical Response of Simulated Semi-Crystalline Polymeric Materials," *Materials Science Forum*, vol. 514–516, pp. 810–814, May 2006, doi: 10.4028/www.scientific.net/MSF.514-516.810.

[30] A. Terteci-Popescu and T. A. Beu, "Branched polyethyleneimine: CHARMM force field and molecular dynamics simulations," *J. Comput. Chem.*, vol. 43, no. 31, pp. 2072–2083, Dec. 2022, doi: 10.1002/jcc.27005.

[31] J. Han and R. H. Boyd, "Small-Molecule Penetrant Diffusion in Hydrocarbon Polymers As Studied by Molecular Dynamics Simulation," *Macromolecules*, vol. 27, no. 19, pp. 5365–5370, Sep. 1994, doi: 10.1021/ma00097a016.

[32] A. Patidar and G. Goel, "MARTINI Coarse-grained Force Field for Thermoplastic Starch Nanocomposites," *Journal of Physical Chemistry B*, vol. 128, no. 46, pp. 11468–11480, Jun. 2024, doi: 10.1021/acs.jpcb.4c05637.

[33] J. Brandrup, E. Immergut, and E. A. HGrulke, *Polymer handbook*, 4th ed. John Wiley and Sons, 1999.

[34] W. L. Jorgensen, D. S. Maxwell, and J. Tirado-Rives, "Development and Testing of the OPLS All-Atom Force Field on Conformational Energetics and Properties of Organic Liquids," *J. Am. Chem. Soc.*, vol. 118, no. 45, pp. 11225–11236, Nov. 1996, doi: 10.1021/ja9621760.

[35] D. W. Van Krevelen and K. Te Nijenhuis, *Properties Polymer their Correlation with Chemical Structure: Their Numerical Estimation and Prediction from Additive Group Contributions*, 4th ed. 2008.

[36] D. Rigby and R.-J. Roe, "Molecular dynamics simulation of polymer liquid and glass. I. Glass transition," *J. Chem. Phys.*, vol. 87, no. 12, pp. 7285–7292, Dec. 1987, doi: 10.1063/1.453321.

[37] M. Gilbert and S. Patrick, "Poly(Vinyl Chloride)," in *Brydson's Plastics Materials*, 8th ed., Elsevier Inc., 2017, pp. 329–388. doi: 10.1016/B978-0-323-35824-8.00013-X.

[38] P. J. Steinbach and B. R. Brooks, "New spherical-cutoff methods for long-range forces in macromolecular simulation," *J. Comput. Chem.*, vol. 15, no. 7, pp. 667–683, Jul. 1994, doi: 10.1002/jcc.540150702.

[39] R. W. Hockney and J. W. Eastwood, *Computer Simulation Using Particles*, 1st ed. Taylor & Francis, 1988. doi: 10.1201/9780367806934.

[40] Y. K. Choi *et al.*, "CHARMM-GUI Polymer Builder for Modeling and Simulation of Synthetic Polymers," *J. Chem. Theory Comput.*, vol. 17, no. 4, pp. 2431–2443, Apr. 2021, doi: 10.1021/acs.jctc.1c00169.

[41] N. S. Alghunaim, "Spectroscopic analysis of PMMA/PVC blends containing CoCl2," *Results Phys.*, vol. 5, pp. 331–336, 2015, doi: 10.1016/j.rinp.2015.11.003.

[42] A. E. Amobonye, P. Bhagwat, S. Singh, and S. Pillai, "Biodegradability of Polyvinyl chloride," *Biodegradability of Conventional Plastics: Opportunities, Challenges, and Misconceptions*, pp. 201–220, Jan. 2023, doi: 10.1016/B978-0-323-89858-4.00017-8.

[43] S. Plimpton, "Fast Parallel Algorithms for Short-Range Molecular Dynamics," *J. Comput. Phys.*, vol. 117, no. 1, pp. 1–19, Mar. 1995, doi: 10.1006/JCPH.1995.1039.

[44] W. G. Hoover, "Canonical dynamics: Equilibrium phase-space distributions," *Phys. Rev. A (Coll. Park).*, vol. 31, no. 3, pp. 1695–1697, Mar. 1985, doi: 10.1103/PhysRevA.31.1695.

[45] S. Nosé, "A unified formulation of the constant temperature molecular dynamics methods," *J. Chem. Phys.*, vol. 81, no. 1, pp. 511–519, Jul. 1984, doi: 10.1063/1.447334.

[46] A. Stukowski, "Visualization and analysis of atomistic simulation data with OVITO–the Open Visualization Tool," *Model. Simul. Mat. Sci. Eng.*, vol. 18, no. 1, p. 015012, Jan. 2010, doi: 10.1088/0965-0393/18/1/015012.

[47] K. Binder and W. Kob, *Glassy Materials and Disordered Solids*. WORLD SCIENTIFIC, 2011. doi: 10.1142/7300.

[48] L. Pauling, *The Nature of the Chemical Bond—An Introduction to Modern Structural Chemistry*, 3rd ed. Cornell University Press, 1960.

[49] Lide. D. R., Ed., *Handbook of Chemistry and Physics*, 84th ed. CRC Press, 2004.

[50] L. Monticelli and D. P. Tieleman, "Force Fields for Classical Molecular Dynamics," 2013, pp. 197–213. doi: 10.1007/978-1-62703-017-5_8.

[51] Y. Shi and M. L. Falk, "Strain Localization and Percolation of Stable Structure in Amorphous Solids," *Phys. Rev. Lett.*, vol. 95, no. 9, Aug. 2005, doi: 10.1103/PHYSREVLETT.95.095502.

[52] J. Rottler and M. O. Robbins, "Shear yielding of amorphous glassy solids: Effect of temperature and strain rate," *Phys. Rev. E*, vol. 68, no. 1, p. 011507, Jul. 2003, doi: 10.1103/PhysRevE.68.011507.

[53] J. Johnsen, A. H. Clausen, F. Grytten, A. Benallal, and O. S. Hopperstad, "A thermo-elasto-viscoplastic constitutive model for polymers," *J. Mech. Phys. Solids*, vol. 124, pp. 681–701, Mar. 2019, doi: 10.1016/j.jmps.2018.11.018.

[54] B. Wernisch, M. Al Otmi, E. Beauvais, and J. Sampath, "Evolution of free volume elements in amorphous polymers undergoing uniaxial deformation: a molecular dynamics simulations study," *Mol. Syst. Des. Eng.*, vol. 9, no. 2, pp. 214–225, 2024, doi: 10.1039/D3ME00148B.

[55] H. Eyring, "Viscosity, Plasticity, and Diffusion as Examples of Absolute Reaction Rates," *J. Chem. Phys.*, vol. 4, no. 4, pp. 283–291, Apr. 1936, doi: 10.1063/1.1749836.

[56] Y. Filanova, J. Hauptmann, F. Längler, and K. Naumenko, "Inelastic Behavior of Polyoxymethylene for Wide Strain Rate and Temperature Ranges: Constitutive Modeling and Identification," *Materials*, vol. 14, no. 13, p. 3667, Jul. 2021, doi: 10.3390/ma14133667.

[57] R. S. Hoy and M. O. Robbins, "Strain hardening in bidisperse polymer glasses: Separating the roles of chain orientation and interchain entanglement," *J. Chem. Phys.*, vol. 131, no. 24, Dec. 2009, doi: 10.1063/1.3276800.

[58] R. B. Dupaix and M. C. Boyce, "Constitutive modeling of the finite strain behavior of amorphous polymers in and above the glass transition," *Mechanics of Materials*, vol. 39, no. 1, pp. 39–52, Jan. 2007, doi: 10.1016/j.mechmat.2006.02.006.

[59] R. S. Hoy and M. O. Robbins, "Strain hardening of polymer glasses: Effect of entanglement density, temperature, and rate," *J. Polym. Sci. B Polym. Phys.*, vol. 44, no. 24, pp. 3487–3500, Dec. 2006, doi: 10.1002/polb.21012.

University of Aden Journal of Natural and Applied Sciences., vol.30(1) (2026) 109 – 128

مجلة جامعة عدن للعلوم الطبيعية والتطبيقية

Journal homepage: https://uajnas.adenuniv.com

بحث علمي

نمذجة السلوك الميكانيكي المنشط حرارياً لمادة البولي فينيل كلوريد (PVC)

يسرى فضل علي قاسم[1] و نديم محمد مسهور[2]

1. قسم الفيزياء، كلية التربية - عدن، جامعة عدن، اليمن
2. قسم الفيزياء، كلية العلوم، جامعة عدن، اليمن

https://doi.org/10.47372/uajnas.2026.n1.a07

الملخص

قُعد بولي فينيل كلوريد غير الملدن (uPVC) من اللدائن الحرارية الإنشائية بالغة الأهمية، حيث تتأثر استجاباته الميكانيكية العيانية (macroscopic) بعمق بالديناميكا الذرية التي لا تزال تمثل تحدياً في توصيفها من خلال الطرق التجريبية التقليدية. في هذا الدراسة، تم فحص الاستجابة الميكانيكية لمركب uPVCغير البلوري لتوفير رؤى على المستوى الجزيئي حول سلوكه العياني. أُجريت عمليات محاكاة للديناميكا الجزيئية (Molecular Dynamics) الذرية باستخدام حزمة LAMMPS مع حقل قوة CHARMM مُعاد المعايرة. وتم موازنة الأنظمة غير البلورية عبر بروتوكول حراري صارم متعدد المراحل ضمن نظام NPT للوصول إلى كثافة متقاربة قدرها 1.345 جم/سم³، تلا ذلك إجراء اختبارات شد أحادية المحور عند معدل انفعال ثابت قدره 5×10^9 ثانية$^{-1}$.

وقد لوحظ أن رفع درجة الحرارة من 200 كلفن إلى 350 كلفن أدى إلى خفض إجهاد الخضوع بشكل منهجي من حوالي 250 ميجا باسكال إلى 100 ميجا باسكال، كما قلل بشكل كبير من صلابة المادة. علاوة على ذلك، كشف التحليل الكمي لنصف قطر الدوران، ومعامل هيرمان للتوجيه، والحجم الحر الجزئي أنه بينما يكون التشوه المرن الأولي مدفوعاً بالمحتوى الحراري نتيجة التفاعلات الجزيئية غير المرتبطة، فإن التصلب عند الانفعالات الكبيرة يكون مدفوعاً بالعشوائية، وتحكمه عملية فك السلاسل والمحاذاة القطاعية بشكل ملحوظ. وتؤكد هذه النتائج أن الطاقة الحرارية المرتفعة تسهل الحركية الجزيئية، مما يؤدي إلى خفض حواجز الطاقة للتحولات التشكيلية وينتج عنه تحولات طاقية أكثر سلاسة مقارنة بالمقاومة الصلبة الملحوظة عند درجات الحرارة المنخفضة. وبناءً على ذلك، توضح هذه الدراسة فاعلية إطار الديناميكا الجزيئية في ربط الطوبولوجيا الجزيئية بالأداء اللزوجي المرن العياني، مما يقدم مساهمة جوهرية في فهم أسطح الخضوع للبوليمرات والآليات الأساسية التي تحكم اللدائن الحرارية الزجاجية.

مفاتيح البحث

التسليم: 30/ 04 / 2026
القبول : 09 / 08 / 2026

كلمات مفتاحية:

محاكاة الديناميكا الجزيئية
بولي فينيل كلوريد غير الملدن (uPVC)،
الخواص الميكانيكية،
حقل قوة CHARMM